

Cross-modal Full-mode Fine-grained Alignment for Text-to-Image Person Retrieval

HAO YIN and XIN MAN, Shenzhen Institute for Advanced Study, University of Electronic Science and Technology of China, China

FEIYU CHEN, JIE SHAO*, and HENG TAO SHEN, Sichuan Artificial Intelligence Research Institute, China University of Electronic Science and Technology of China, China

Text-to-Image Person Retrieval (TIPR) is a cross-modal matching task that aims to retrieve the most relevant person images based on a given text query. The key challenge in TIPR lies in achieving effective alignment between textual and visual modalities within a common latent space. To address this challenge, prior approaches incorporate attention mechanisms for implicit cross-modal local alignment. However, they lack the ability to verify whether all local features are correctly aligned. Moreover, existing methods primarily focus on hard negative samples during model updates, with the goal of refining distinctions between positive and negative pairs, often neglecting incorrectly matched positive pairs. To alleviate these issues, we propose FMFA, a cross-modal Full-Mode Fine-grained Alignment framework, which enhances global matching through explicit fine-grained alignment and existing implicit relational reasoning—hence the term “full-mode”—without requiring additional supervision. Specifically, we design an Adaptive Similarity Distribution Matching (A-SDM) module to rectify unmatched positive sample pairs. A-SDM adaptively pulls the unmatched positive pairs closer in the joint embedding space, thereby achieving more precise global alignment. Additionally, we introduce an Explicit Fine-grained Alignment (EFA) module, which makes up for the lack of verification capability of implicit relational reasoning. EFA strengthens explicit cross-modal fine-grained interactions by sparsifying the similarity matrix and employs a hard coding method for local alignment. Our proposed method is evaluated on three public datasets, achieving state-of-the-art performance among all global matching methods. Our code is available at <https://github.com/yinhao1102/FMFA>.

CCS Concepts: • **Information systems** → **Image search**; • **Computing methodologies** → *Object identification*.

Additional Key Words and Phrases: Cross-modal retrieval, Person search, Fine-grained alignment

ACM Reference Format:

Hao Yin, Xin Man, Feiyu Chen, Jie Shao, and Heng Tao Shen. 2025. Cross-modal Full-mode Fine-grained Alignment for Text-to-Image Person Retrieval. *ACM Trans. Multimedia Comput. Commun. Appl.* 1, 1, Article 1 (January 2025), 20 pages. <https://doi.org/XXXXXX.XXXXXXX>

1 Introduction

Text-to-Image Person Retrieval (TIPR) aims to comprehend natural language descriptions and retrieve the most relevant person image from a large image gallery [27]. Unlike general image-text

*Corresponding author.

Authors' Contact Information: Hao Yin, yinhao1102@std.uestc.edu.cn; Xin Man, manxin@std.uestc.edu.cn, Shenzhen Institute for Advanced Study, University of Electronic Science and Technology of China, Shenzhen, China; Feiyu Chen, chenfeiyu@uestc.edu.cn; Jie Shao, shaojie@uestc.edu.cn; Heng Tao Shen, shenhengtao@hotmail.com, Sichuan Artificial Intelligence Research Institute, Yibin, China and University of Electronic Science and Technology of China, Chengdu, China.

Permission to make digital or hard copies of all or part of this work for personal or classroom use is granted without fee provided that copies are not made or distributed for profit or commercial advantage and that copies bear this notice and the full citation on the first page. Copyrights for components of this work owned by others than the author(s) must be honored. Abstracting with credit is permitted. To copy otherwise, or republish, to post on servers or to redistribute to lists, requires prior specific permission and/or a fee. Request permissions from permissions@acm.org.

© 2025 Copyright held by the owner/author(s). Publication rights licensed to ACM.

ACM 1551-6865/2025/1-ART1

<https://doi.org/XXXXXX.XXXXXXX>

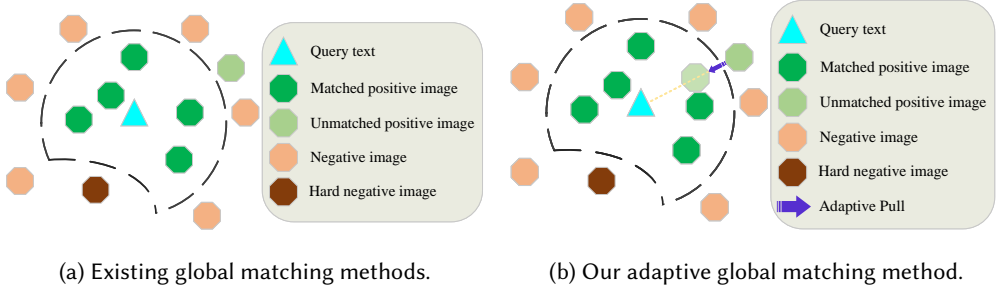


Fig. 1. Evolution of global matching methods for text-to-image person retrieval. (a) Existing global matching methods focus on hard negative samples to learn a discriminative boundary in a common latent space, thus enhancing the distinction between positive and negative samples. (b) Our adaptive global matching method builds on a discriminative boundary and concentrates on unmatched positive samples, adaptively pulling them closer to the corresponding query text.

retrieval [5, 6, 40], which tends to achieve semantic-based matching between text and image, TIPR is specifically designed for identifying individuals. TIPR requires the accurate modeling of fine-grained correspondences between textual and visual modalities, owing to the large intra-class variance and small inter-class difference. This substantial intra-class variation arises from two aspects: (1) visual appearances of the same identity exhibit dramatic variations under different poses, viewpoints, and illumination conditions, and (2) textual descriptions are influenced by differences in phrasing, word order and textual ambiguities. Therefore, the primary challenges in TIPR are how to extract discriminative global representations from image-text pairs and how to achieve precise cross-modal fine-grained alignment. Existing methods for tackling these challenges can be roughly divided into two main categories: global matching methods and local matching methods.

Some global matching methods [51, 52] obtain discriminative global representations by aligning images and texts, which are projected into a joint embedding space. Their commonly used loss functions include the Cross-Modal Projection Matching (CMPPM) loss [51] and the Similarity Distribution Matching (SDM) loss [17]. The CMPPM loss focuses on the difference between the scalar projection of image-text pairs and their corresponding matching labels. In comparison, the SDM loss enhances global image-text matching by minimizing the Kullback-Leibler (KL) divergence between the normalized similarity score distribution of image-text pairs and the ground-truth label distribution. In addition, the SDM loss incorporates a temperature hyperparameter to make model updates concentrate on hard negative samples, yet it leads to the neglect of unmatched positive pairs, as shown in Figure 1a. However, in TIPR, the accurate matching of positive pairs is prioritized over merely distinguishing between positive and negative pairs. Meanwhile, some local matching methods [2, 9, 31] incorporate attention mechanisms to achieve cross-modal fine-grained alignment. For instance, RaSa [2] constructs a cross-modal encoder to generate multimodal representations for subsequent fine-grained alignment. Building on RaSa, MARS [9] integrates an MAE decoder [12] to reconstruct masked image patch sequences into their original unmasked form, thereby facilitating cross-modal fine-grained alignment. However, these methods rely on attention mechanisms to implicitly aggregate local image-text representations. As a result, they yield only the final multimodal representation, without revealing the details of the aggregation process. Consequently, these implicit aggregation methods make it difficult to determine whether the aggregated multimodal representations correctly encode the corresponding visual and textual information.

To overcome these issues, we introduce **FMFA**, a **cross-modal Full-Mode Fine-grained Alignment framework**, which enhances global matching through full-mode fine-grained alignment, including explicit fine-grained image-text alignment and existing implicit relational reasoning. Specifically, we design an **Adaptive Similarity Distribution Matching (A-SDM)** module to ensure the correct matching of positive image-text pairs. Within the joint embedding space, the A-SDM module adaptively pulls positive pairs closer together. In cases of mismatched positive pairs, the A-SDM module adaptively regulates the pulling force based on their relative distance within the joint embedding space, as shown in Figure 1b, thus improving cross-modal global alignment. Inspired by the observation that multiple image patches usually correspond to one word in the caption [3], we introduce an **Explicit Fine-Grained Alignment (EFA)** module. The EFA module derives multimodal representations through explicit aggregation with a sparse similarity matrix. During this process, the sparse similarity matrix between text and image reflects the contribution of textual and visual representations to the final multimodal representation. To minimize redundancy and reduce the computational cost during training, the EFA module employs hard coding alignment between the aggregated multimodal representation and its original visual and textual representations. These designs enable EFA to achieve cross-modal fine-grained interactions and help the backbone network to extract more discriminative global image-text representations without requiring additional supervision. FMFA is evaluated on three public benchmarks [8, 23, 53], and it achieves state-of-the-art performance while maintaining high inference speed. Our main contributions are summarized as follows:

- We propose FMFA to explicitly exploit fine-grained interactions to enhance cross-modal alignment without additional supervision and inference cost.
- We introduce an adaptive similarity distribution matching module, which is designed to accurately align image-text pairs within a joint embedding space. It adaptively adjusts to narrow the distance between mismatched positive pairs, ensuring more precise matching.
- We develop an explicit fine-grained alignment module, which leverages the sparse similarity matrix for explicit aggregation and employs a hard coding method in cross-modal fine-grained alignment to minimize redundant information.

2 Related Work

Text-to-Image Person Retrieval (TIPR) was first introduced by Li et al. [23], who constructed the CUHK-PEDES dataset. The core challenge of TIPR is to learn a common latent space where visual and textual representations are well aligned. Existing methods can be broadly categorized into global and local matching approaches.

Early global methods [39, 52, 53] directly aligned the global representations of images and text in a joint embedding space. Schroff et al. [35] proposed a triplet ranking loss to enforce a margin constraint between positive and negative pairs, and Zhang et al. [51] introduced the CMPM/C loss to minimize the discrepancy between the scalar projection of image-text pairs and their labels. However, these global methods lack cross-modal fine-grained interactions, which restrict their ability to capture detailed semantic correspondences. To address this limitation, early local matching methods [10, 38, 44] explicitly aligned local visual and textual features to achieve fine-grained cross-modal interactions. Nevertheless, they rely on unimodal pre-trained models (e.g., BERT [7] and ResNet [13]), failing to exploit the strong cross-modal alignment capability of recent pre-trained Vision-Language Models (VLMs) [21, 22, 47].

Recent local matching methods [9, 15, 28, 32, 46] have benefited greatly from VLMs and introduced VLMs to enhance cross-modal alignment. Park et al. [31] utilized a modified Contrastive Language-Image Pre-training (CLIP) [33] model as the feature extractor and designed a slot attention-based [26]

part discovery module to identify discriminative human parts without extra supervision, while Bai et al. [2] used the align-before-fuse model [22] as the backbone and introduced a cross-modal encoder for fine-grained alignment. Although effective, these methods involve complex computations during inference, leading to high time and memory costs, which limit their applicability to real-time systems.

On another line of research, several studies [37, 41, 49] have explored leveraging large-scale image-text pairs in the person Re-IDentification (ReID) domain to VLMs. Zuo et al. [54] utilized CUHK-PEDES and ICFG-PEDES to train an image captioner, aiming to generate comprehensive textual descriptions for pedestrian images. Yang et al. [49] employed BLIP-2 [20] to produce attribute-aware captions for diffusion-generated pedestrian images [34], while Jiang et al. [18] leveraged recent multi-modal large language models (MLLMs), such as Qwen-VL [1] and LLaVA [24], to automatically annotate large-scale ReID datasets in a human-like manner. The CLIP models pre-trained on large-scale ReID datasets exhibit strong zero-shot performance. Their compatibility with global matching methods—which relies solely on global features and has a simple inference pipeline—makes them particularly suitable for direct fine-tuning in such settings.

Among the global matching methods, IRRA [17] recently attempted to enhance fine-grained interactions by introducing an Implicit Relation Reasoning (IRR) module, utilizing attention mechanisms to capture cross-modal relations. However, this implicit alignment cannot guarantee that all corresponding local features are correctly matched. In light of these limitations, we propose FMFA, which aims to enhance the global matching ability of the model by achieving cross-modal full-mode fine-grained alignment, including explicit fine-grained alignment and implicit relation reasoning.

3 Method

In this section, we present our proposed FMFA framework. The overview of FMFA is illustrated in Figure 2 and the details are introduced in the following subsections.

3.1 Feature Extraction

Inspired by the success of IRRA [17], we use the modified full CLIP [33] visual and textual encoders to enhance cross-modal alignment capabilities while reducing inference costs.

Visual Modality. Given an input image $I \in R^{H \times W \times C}$, a CLIP pre-trained ViT model is adopted to obtain the image embeddings. We first split I into a sequence of $N = H \times W / P^2$ fixed-sized non-overlapping patches, where P denotes the patch size, and then map the patch sequences to 1D tokens $\{f_i^v\}_{i=1}^N$ by a trainable linear projection. With the injection of the positional embedding and the extra [CLS] token, the sequence of tokens $\{f_{cls}^v, f_1^v, \dots, f_N^v\}$ are input into L -layer transformer blocks to model the correlations of each patch. Finally, a linear projection is adopted to map f_{cls}^v to the joint image-text embedding space, which serves as the global image representation.

Textual Modality. For an input text T , we directly use the CLIP-Xformer textual encoder [33] to extract the text embeddings. Following CLIP, the lower-cased byte pair encoding [36] is firstly employed to tokenize the input text description. The text description is enclosed with [SOS] and [EOS] tokens to indicate the start and end of the sequence. The tokenized text $\{f_{sos}^t, f_1^t, \dots, f_{eos}^t\}$ is then fed into the textual encoder and exploits the correlations of each patch by masked self-attention. The output of the highest layer of the transformer at the [EOS] token, f_{eos}^t , is linearly projected into the image-text joint embedding space to obtain the global text representation.

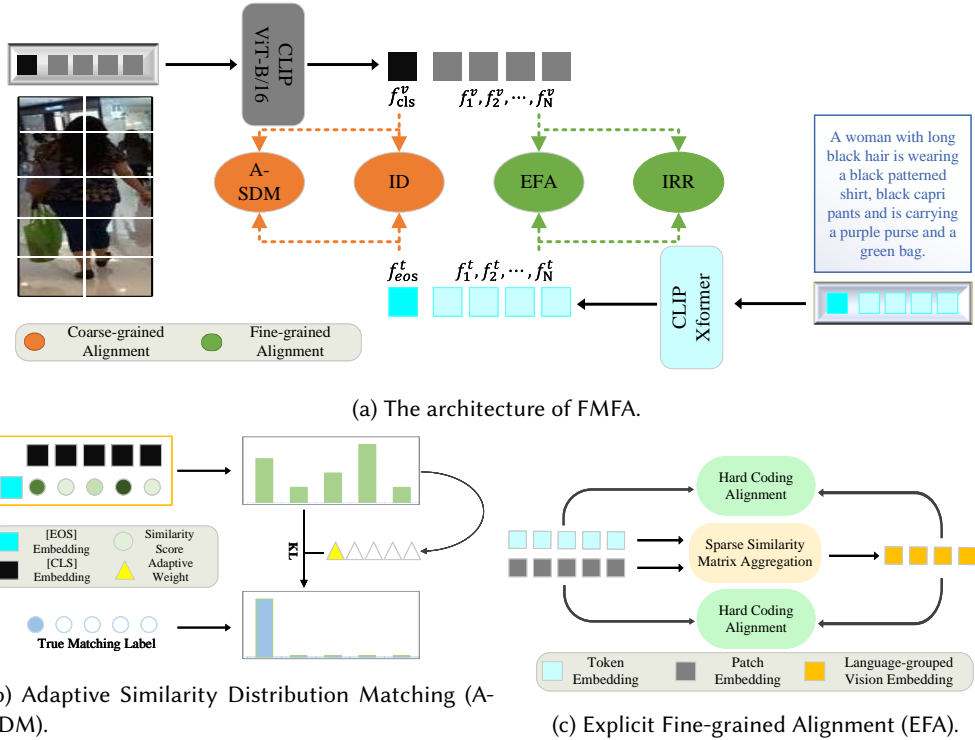


Fig. 2. Overview of the proposed FMFA framework. (a) Our FMFA consists of a dual-stream feature extraction backbone and four representation learning branches, i.e. Identity Identification (ID loss), Adaptive Similarity Distribution Matching (A-SDM), Explicit Fine-grained Alignment (EFA) and Implicit Relation Reasoning (IRR). The former two are coarse-grained alignment modules and the latter two are fine-grained alignment modules. Modules connected by dashed lines will be removed during inference stage. (b) A-SDM obtains the adaptive weight through the similarity score of unmatched positive pairs, adaptively pulling positive pairs closer and dynamically adjusting the pulling force. (c) EFA achieves fine-grained interaction by hard coding alignment of token or patch embeddings and their corresponding language-grouped vision embedding, which is derived from an aggregated sparse similarity matrix.

3.2 Adaptive Similarity Distribution Matching

Adopted from IRRA [17], we introduce a novel Adaptive Similarity Distribution Matching (A-SDM) module, which aims to adaptively pull the unmatched positive image-text pairs into a joint embedding space, thereby enhancing the cross-modal global matching capability of model.

Given a mini-batch of B image-text pairs, for each global text representation g_i^t and global image representation g_j^v , we construct a set of image-text representation pairs as $\{(g_i^t, g_j^v), y_{i,j}\}_{j=1}^N$, where $y_{i,j}$ is the matching label. $y_{i,j} = 1$ means that (g_i^t, g_j^v) is a matched pair, while $y_{i,j} = 0$ means that (g_i^t, g_j^v) is an unmatched pair. Let $\cos(\mathbf{u}, \mathbf{v}) = \mathbf{u}^\top \mathbf{v} / \|\mathbf{u}\| \|\mathbf{v}\|$ denotes the cosine similarity of u and v . Then, the similarity matrix of matching pairs can be simply calculated by the following softmax function:

$$p_{i,j} = \frac{\exp(\cos(g_i^t, g_j^v) / \tau_1)}{\sum_{k=1}^N \exp(\cos(g_i^t, g_k^v) / \tau_1)}, \quad (1)$$

where τ_1 is a temperature hyperparameter which controls the probability distribution peaks. The matching probability $p_{i,j}$ can be viewed as the proportion of the cosine similarity score between g_i^t and g_j^v to the sum of cosine similarity scores between g_i^t and $\{g_j^v\}_{j=1}^N$ in a mini-batch.

Let the i -th text T_i in the mini-batch be the query text and I_i be the corresponding image for T_i at rank- k , where $k > 1$. Different from IRRA [17], we propose to calculate adaptive weight based on the similarity between the query text T_i and all image representations:

$$w_i^{t2i} = \alpha \cdot \left[\max_k p_{i,k} - p_{i,i} \right] + 1, \quad (2)$$

where α is a weight factor which reflects the contribution of unmatched image-text pairs to the cross-modal global matching capability of the model. $w_i^{t2i} = 1$ indicates that the query text T_i and its corresponding image I_i are successfully matched, while $w_i^{t2i} > 1$ indicates that T_i and I_i are unmatched. The A-SDM loss from text to image within a mini-batch is then computed as:

$$\mathcal{L}_{t2i} = W^{t2i} * KL(\mathbf{p}_i \parallel \mathbf{q}_i) = \frac{1}{B} \sum_{i=1}^B w_i^{t2i} \sum_{j=1}^B p_{i,j} \log\left(\frac{p_{i,j}}{q_{i,j} + \epsilon}\right), \quad (3)$$

where ϵ is a small constant to avoid numerical problems, and $q_{i,j} = y_{i,j} / \sum_{k=1}^B$ is the true matching probability.

Symmetrically, the A-SDM loss from image to text \mathcal{L}_{i2t} can be obtained by exchanging the visual and textual modalities. The bi-directional A-SDM loss is calculated by:

$$\mathcal{L}_{A-sdm} = \mathcal{L}_{i2t} + \mathcal{L}_{t2i}. \quad (4)$$

3.3 Explicit Fine-grained Alignment

To fully exploit fine-grained information, it is crucial to bridge the inherent modality differences between visual and textual modalities. Although most existing fine-grained alignment methods based on attention mechanisms have achieved certain results by implicitly aligning local features of images and texts, they cannot directly observe whether the corresponding local features of image and text are effectively aligned. We introduce an explicit cross-modal aggregation method based on the sparse similarity matrix between the image and text local features. To further reduce redundant information and minimize memory and time costs during fine-grained alignment, we use hard coding to align the aggregated language-grouped vision embeddings with both image and text embeddings, as shown in Figure 2c.

Sparse Similarity Matrix Aggregation. Some methods [29, 50] use loss functions based on fine-grained representations for cross-modal local alignment, which compute the similarity between all image patch embeddings and text token embeddings. Obviously, this approach is computationally and memory-intensive, making it difficult to scale to large batches. Therefore, some methods attempt to sparsify the full-size similarity matrix and only consider the retrieved embeddings that are similar to the query embedding. Most sparse processing methods are based on softmax, but the softmax approach tends to produce a low-entropy distribution from the perspective of gradient flow [14]. Therefore, we implement sparse similarity matrix aggregation using max-min normalization.

An image I and its corresponding text T are fed into the visual encoder and textual encoder, respectively, as described in Section 3.1. As illustrated in Figure 3a, the similarity between all image patches and text tokens is obtained by computing the inner product of the last hidden states $\{f_i^t\}_{i=1}^L$ and $\{f_i^v\}_{i=1}^N$ of the text transformer and the vision transformer. $s_{i,j} = f_i^t \cdot f_j^v$ represents the similarity between the text token f_i^t and the image patch f_j^v , where \cdot denotes the inner product. To obtain the aggregation weight, for each token i , we first normalize $s_{i,j}$ to $[0,1]$ using the following min-max

normalization formula:

$$\hat{s}_{i,j} = \frac{s_{i,j} - \min_k s_{i,k}}{\max_k s_{i,k} - \min_k s_{i,k}}. \quad (5)$$

We sparsify the normalized similarity matrix to encourage cross-modal interactions between each token and its patches with higher similarity:

$$\tilde{s}_{i,j} = \begin{cases} \hat{s}_{i,j} & \text{if } \hat{s}_{i,j} \geq \sigma \\ 0 & \text{otherwise} \end{cases}, \quad (6)$$

where σ is the sparsity threshold. σ is set to $1/N$, where N is the number of image patches. This ensures that each token has a minimum of one corresponding image patch for alignment. We compute the aggregation weights by:

$$agg_{i,j} = \frac{\tilde{s}_{i,j}}{\sum_{m=1}^M \tilde{s}_{i,j}}, \quad (7)$$

where M is the number of image patches retained with high similarity to the token i , and $agg_{i,j}$ represents the weight of patch j for aggregating the language-grouped vision embedding corresponding to token i . This explicit aggregation strategy ensures a comprehensive interaction between token i and its corresponding patch j during local alignment. In particular, the aggregation weight $agg_{i,j}$ effectively captures the semantic relevance between token i and patch j , thereby facilitating precise alignment.

Then, we obtain the corresponding language-grouped vision embedding e_i as follows:

$$e_i = \sum_{j=1}^N agg_{i,j} \cdot f_j^v, \quad (8)$$

where N denotes the number of image patches. The resulting set of language-grouped vision embedding e_i has the same length L as the text token f_i^t .

Hard Coding Alignment. We calculate the similarity between the language-grouped vision embeddings (referred to as joint embeddings) $\{e_i\}_{i=1}^L$ and their corresponding original text embeddings $\{f_i^t\}_{i=1}^L$ as well as image embeddings $\{f_i^v\}_{i=1}^N$, respectively. To reduce both computational and memory costs, we adopt a hard coding similarity computation between the joint embeddings and their corresponding text and image embeddings. For simplicity, we only present the calculation between the joint embeddings and the text embeddings, while the remaining computations follow a similar and symmetric approach.

For the text T and its corresponding joint embedding E , we calculate the original similarity matrix O between all text tokens $\{f_i^t\}_{i=1}^L$ and their joint embeddings $\{e_i\}_{i=1}^L$, where $o_{i,j} = f_i^t e_j^{\top} / \|f_i^t\| \|e_j\|$ means the cosine similarity of f_i^t and e_j . For the token f_i^t , we compute the weight factor between it and all joint embeddings using the following hard coding way:

$$\omega_{i,j} = \begin{cases} 1 & \text{if } j = \operatorname{argmax}_{j'=1 \cdots L} (o_{i,j'}) \\ 0 & \text{otherwise} \end{cases}. \quad (9)$$

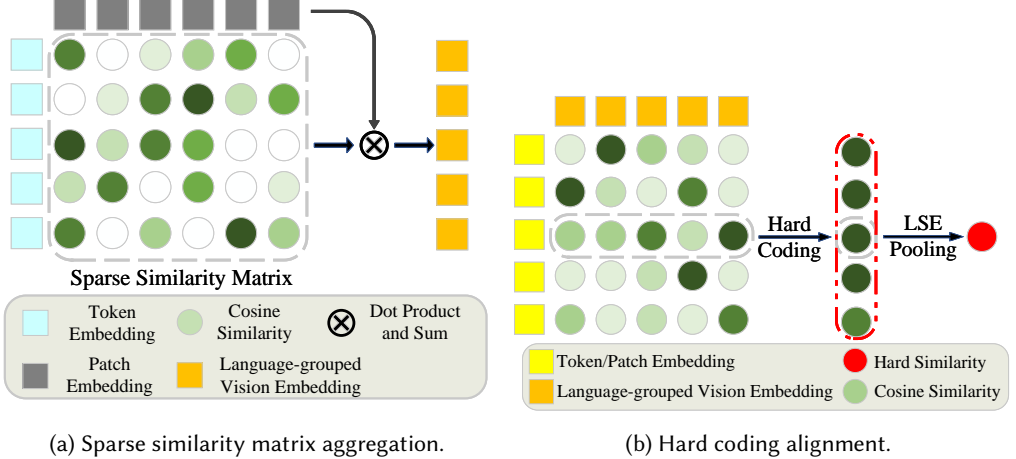


Fig. 3. Illustration of the EFA module. (a) EFA sparsifies the similarity matrix between token embeddings and patch embeddings, and obtains the language-grouped vision embeddings by aggregating the sparse similarity with its corresponding patch. (b) EFA obtains hard similarity through hard coding and LSE pooling, where the calculated hard similarity reflects the relationship between the language-grouped vision embeddings and their original token or patch embeddings.

Then, we utilize the LSE pooling [19] to compute the hard similarity between text T and its corresponding joint embedding E by:

$$\begin{aligned} \text{hard_s}(T, E) &= \text{LSE - Pooling} \left(\sum_{j=1}^L \omega_{i,j} o_{i,j} \right) \\ &= \frac{1}{\lambda} \log \sum_{i=1}^L \exp \left(\lambda \max_{j=1 \dots L} o_{i,j} \right), \end{aligned} \quad (10)$$

where λ is a factor that determines how much to magnify the importance of the most relevant pairs of text embedding and its corresponding joint embedding.

Given a mini-batch of B texts and its corresponding joint embeddings, we obtain the hard coding similarity matrix Hard_S according to Eq. (9) and Eq. (10), as illustrated in Figure 3b. We calculate the EFA loss from the text to its joint embedding, adapted from the triplet ranking loss [35]:

$$\mathcal{L}_{t2e} = \frac{1}{B} \log \sum_{\text{neg}} \exp \left(\frac{\text{Hard_S}_{\text{neg}} - \text{Hard_S}_{\text{pos}} + \text{margin}}{\tau_2} \right), \quad (11)$$

where τ_2 is a temperature hyperparameter that controls the distribution of the loss, and margin is a distance hyperparameter representing the minimum distance difference between positive and negative samples.

Similarly, the EFA loss from the joint embedding to its original text can be computed following Eq. (11), and we can calculate the EFA loss between image and its joint embedding according to Eq. (9), Eq. (10) and Eq. (11). Then, we obtain the full EFA loss by:

$$\mathcal{L}_{\text{efa}} = \mathcal{L}_{t2e} + \mathcal{L}_{e2t} + \mathcal{L}_{i2e} + \mathcal{L}_{e2i}. \quad (12)$$

Theoretical analysis of hard coding: Given visual embeddings of an image $V \in \mathbb{R}^{N \times d}$ and its joint embeddings $E \in \mathbb{R}^{L \times d}$, where N is the number of image patches and L is the length of the

joint embeddings, both the hard coding method and the soft coding method calculate the similarity matrix A to obtain the final similarity between V and E , which requires the same time complexity $O(NLd)$. When processing the similarity matrix A , our hard coding method calculates the maximum similarity for each row, which has a time complexity of $O(N)$, as described in Eq. (9) and Eq. (10). However, the soft coding method processes all similarities, resulting in a time complexity of $O(NL)$. Moreover, the spatial complexity of the hard coding method is $O(NL)$, which is significantly lower than the spatial complexity of the soft coding method, $O(Ld)$. This is based on the fact that $N \ll d$. Therefore, our hard coding method can effectively reduce the cost of training time and memory.

3.4 Training Objective

As mentioned, the primary goal of FMFA is to enhance the global and cross-modal local alignment of image-text representations within the joint embedding space. To achieve it, the most commonly used ID loss [52] and IRR loss [17], together with the proposed EFA loss and the A-SDM loss, are jointly employed to optimize FMFA. The ID loss directly classifies the global features extracted from each image and text according to their identities, thereby enhancing the global alignment of the model. The IRR loss, based on the Masked Language Modeling (MLM) task [42], leverages an attention mechanism for implicit cross-modal interaction to obtain a joint embedding, and then predicts the [MASK] text token to enhance the local alignment of the model.

FMFA is trained in an end-to-end manner and the overall training objective is defined as:

$$\mathcal{L} = \mathcal{L}_{id} + \mathcal{L}_{irr} + \mathcal{L}_{efa} + \mathcal{L}_{A\text{-}sdm}. \quad (13)$$

4 Experiments

4.1 Datasets and Settings

In this section, we present the datasets, evaluation metrics and implementation details in our experiments.

Datasets. We use the CHUK-PEDES [23], ICFG-PEDES [8], and RSTPReid [53] datasets to train and evaluate our FMFA. We follow the data partitions used in IRRA [17] to split each dataset into training, validation and test sets, where the ICFG-PEDES dataset only has training and validation sets.

- CUHK-PEDES is the first benchmark specifically designed for text-to-image person retrieval. It comprises 40,206 images and 80,412 textual descriptions corresponding to 13,003 identities. According to the official split, the training set includes 11,003 identities, with 34,054 images and 68,108 descriptions. The validation and test sets contain 3,078 and 3,074 images, as well as 6,158 and 6,156 textual descriptions, respectively, each covering 1,000 distinct identities.
- ICFG-PEDES consists of 54,522 images corresponding to 4,102 identities, with each image paired with a single textual description. The dataset is split into a training set and a test set: the training set includes 34,674 image-text pairs from 3,102 identities, while the test set comprises 19,848 pairs covering the remaining 1,000 identities.
- RSTPReid comprises 20,505 images of 4,101 identities captured by 15 different cameras. Each identity is associated with 5 images taken from different viewpoints, and each image is annotated with 2 textual descriptions. According to the official split, the training, validation, and test sets contain 3,701, 200, and 200 identities, respectively.

Evaluation Metrics. We mainly employ the popular Rank-K metrics ($K=1, 5, 10$) to measure the retrieval performance. In addition to Rank-K, we also adopt the mean Average Precision (mAP) as an auxiliary retrieval metric to further evaluate performance. Higher evaluation metrics indicate better performance of the model.

Table 1. The margins utilized in the EFA loss. “T. to E.” means the EFA loss from textual embeddings to the corresponding joint embeddings, and “V. to E.” means the EFA loss from visual embeddings to the corresponding joint embeddings.

	CUHK-PEDES	ICFG-PEDES	RSTPReid
T. to E.	0.1	0.2	0.2
V. to E.	0.1	1.0	0.8

Implementation Details. As mentioned in Section 3.1, we employ either the original pre-trained CLIP model [33] or ReID-domain pre-trained variants of CLIP [18, 41] as our modality-specific encoders. For fairness, we use the same version of CLIP-ViT-B/16 as the visual encoder and Xformer as the textual encoder in IRRA [17] to conduct experiments. Specifically, the input size of images is 384×128 and the maximum length L of the input word tokens is set to 77. We employ the Adam optimizer to train our model for 60 epochs with a cosine learning rate decay strategy by default, which differs from the 100 epochs used for the ICFG-PEDES dataset. The initial learning rate is $1e-5$ and the batch size is 64 for the original CLIP model parameters. In particular, the temperature parameter τ_1 in the A-SDM loss is set to 0.02, while the temperature parameter τ_2 in the EFA loss is set to 1.0. The weight parameter α in the A-SDM loss is set to 10.0 by default, and set to 1 in the RSTPReid dataset, and the factor λ in the LSE pooling is set to 1.0. Due to variations in data distribution, the margins used in the EFA loss differ across the three datasets. The specific margins used in Eq. (11) for each dataset are provided in Table 1. When using ReID-domain pre-trained CLIP models, we adopt the same initial learning rate and batch size as in NAM [41] and HAM [18], while keeping all other settings unchanged.

4.2 Comparison with State-of-the-Art Methods

In this section, we present a comparison with state-of-the-art methods (e.g., NAM [41] and HAM [18]) on three public benchmark datasets. Based on the backbone type, we categorize the baselines into two groups, as shown in Table 2, Table 3, and Table 4: those employing VL-Backbones w/o ReID-domain pre-training and with ReID-domain pre-training. Furthermore, according to whether local features are utilized during inference, the baselines are further divided into local matching methods and global matching methods (denoted as “L” and “G” in the “Type” column, respectively). Note that the baseline model in Table 2, Table 3 and Table 4 is denoted as IRRA^R, which represents the performance of our reimplementation of the IRRA model. CLIP refers to the CLIP-ViT-B/16 model fine-tuned with the InfoNCE loss [30].

Performance Comparisons on CUHK-PEDES. We evaluate FMFA on the widely used CUHK-PEDES benchmark, as shown in Table 2. When using the VL-Backbones without ReID-domain pre-training, FMFA outperforms all state-of-the-art global matching methods with 74.16% Rank-1 accuracy and 66.66% mAP, and further exceeds IRRA by 0.74% and 0.41% in Rank-5 and Rank-10, respectively. When adopting the VL-Backbones with ReID-domain pre-training, FMFA maintains its superiority, and achieves Rank-5 accuracy exceeding 95% with the HAM-based backbone. Notably, FMFA with NAM-based backbone attains 91.33% in Rank-5, outperforming IRRA with the HAM-based backbone by 0.13%.

Performance Comparisons on RSTPReid. We evaluate FMFA on the newest benchmark, RSTPReid, as shown in Table 3. Using the VL-Backbones without ReID-domain pre-training, FMFA achieves competitive performance, attaining 61.05% Rank-1, 83.85% Rank-5, 89.80% Rank-10, and 48.22% mAP, respectively, outperforming IRRA by 1.55% in Rank-1 and 2.05% in Rank-5. When adopting the VL-Backbones with ReID-domain pre-training, our method achieves further gains,

Table 2. Performance comparisons with state-of-the-art methods on the CUHK-PEDES dataset. “G”, “L” and “P” in the “Type” column stand for global-matching method, local-matching method and pre-trained model with ReID-domain respectively. “Image Enc.” and “Text Enc.” mean the backbone of image encoder and text encoder respectively. “IRRA^R” means the model that we reproduce.

Type	Method	Ref.	Image Enc.	Text Enc.	Rank-1	Rank-5	Rank-10	mAP
<i>VL-Backbones w/o ReID-domain pre-training:</i>								
G	LGUR [38]	MM22	ResNet50	BERT	65.25	83.12	89.00	-
	IVT [39]	ECCV22	ViT-B/16	BERT	65.59	83.11	89.21	-
	CLIP [33]	ICML21	CLIP-ViT	CLIP-Xformer	68.19	86.47	91.47	61.12
	DM-Adapter [25]	AAAI25	CLIP-ViT	CLIP-Xformer	72.17	88.74	92.85	64.33
	IRRA ^R [17]	CVPR23	CLIP-ViT	CLIP-Xformer	73.45	89.38	93.69	66.13
	TBPS-CLIP [4]	AAAI24	CLIP-ViT	CLIP-Xformer	73.54	88.19	92.35	65.38
	FMFA (ours)		CLIP-ViT	CLIP-Xformer	74.16	90.12	94.10	66.66
L	ACSA [16]	TMM22	Swin-B	BERT	63.56	81.49	87.70	-
	Han et al. [11]	arXiv21	CLIP-RN101	CLIP-Xformer	64.08	81.73	88.19	60.08
	PLOT [31]	ECCV24	CLIP-ViT	CLIP-Xformer	75.28	90.42	94.12	-
	RaSa [2]	IJCAI23	CLIP-ViT	BERT-base	76.51	90.29	94.25	69.38
	PTMI [28]	TIFS25	CLIP-ViT	CLIP-Xformer	76.02	89.93	94.14	70.85
	APTM [49]	MM23	Swin-B	BERT-base	76.53	90.04	94.15	66.91
	SCVD [45]	TCSVT24	CLIP-RN50	CLIP-Xformer	76.72	90.38	94.89	-
<i>VL-Backbones with ReID-domain pre-training:</i>								
P+G	UniPT [37] + IRRA [17]	ICCV23	CLIP-ViT	CLIP-Xformer	74.37	89.51	93.97	66.60
	PLIP [54] + IRRA [17]	NeurIPS24	CLIP-ViT	CLIP-Xformer	74.25	89.49	93.68	66.52
	NAM [41] + IRRA ^R	CVPR24	CLIP-ViT	CLIP-Xformer	76.67	91.11	94.60	68.42
	NAM [41] + FMFA (ours)		CLIP-ViT	CLIP-Xformer	77.23	91.33	94.75	68.53
	HAM [18] + IRRA ^R	CVPR25	CLIP-ViT	CLIP-Xformer	77.32	91.20	94.95	68.87
	HAM [18] + FMFA (ours)		CLIP-ViT	CLIP-Xformer	77.46	91.36	95.01	68.89

Table 3. Performance comparisons with state-of-the-art methods on the RSTPReid dataset.

Type	Method	Rank-1	Rank-5	Rank-10	mAP
<i>VL-Backbones w/o ReID-domain pre-training:</i>					
G	DSSL [53]	39.05	62.60	73.95	-
	IVT [39]	46.70	70.00	78.80	-
	CLIP [33]	54.05	80.70	88.00	43.41
	IRRA ^R [17]	59.50	81.80	88.85	47.44
	DM-Adapter [25]	60.00	82.10	87.90	47.37
	FMFA (ours)	61.05	83.85	89.80	48.22
L	ACSA [28]	48.40	71.85	81.45	-
	CFine [47]	50.55	72.50	81.60	-
	PLOT [31]	61.80	82.85	89.45	-
	RaSa [2]	66.90	86.50	91.35	52.31
	APTM [49]	67.50	85.70	91.45	52.56
	<i>VL-Backbones with ReID-domain pre-training:</i>				
P+G	UniPT [37] + IRRA [17]	62.20	83.30	89.75	48.33
	PLIP [54] + IRRA [17]	64.35	83.75	91.00	50.93
	NAM [41] + IRRA ^R	68.25	86.75	92.30	52.92
	NAM [41] + FMFA (ours)	68.70	87.05	92.35	53.14
	HAM [18] + IRRA ^R	71.35	87.60	93.05	55.40
	HAM [18] + FMFA (ours)	71.80	88.05	93.15	55.72

exceeding IRRA by 0.45% in Rank-1 with both the NAM-based and HAM-based backbones. Notably, FMFA achieves Rank-5 accuracy higher than 88% with the HAM-based backbone.

Performance Comparisons on ICFG-PEDES. We also evaluate FMFA on another benchmark, ICFG-PEDES, as shown in Table 4. Using VL-Backbones without ReID-domain pre-training, FMFA achieves the best performance across all evaluation metrics, attaining 64.29% Rank-1 and 39.43% mAP. Compared with IRRA, FMFA shows a notable improvement of 0.81% in Rank-1 and 1.23% in

Table 4. Performance comparisons with state-of-the-art methods on the ICFG-PEDES dataset.

Type	Method	Rank-1	Rank-5	Rank-10	mAP
<i>VL-Backbones w/o ReID-domain pre-training:</i>					
G	Dual Path [52]	38.99	59.44	68.41	-
	IVT [39]	56.04	73.60	80.22	-
	CLIP [33]	56.74	75.72	82.26	31.84
	DM-Adapter [25]	62.64	79.53	85.32	36.50
	IRRA ^R [17]	63.48	80.16	85.78	38.20
	FMFA (ours)	64.29	80.48	85.93	39.43
L	SSAN [8]	54.23	72.63	79.53	-
	ISANet [48]	57.73	75.42	81.72	-
	CFine [47]	60.83	76.55	82.42	-
	RaSa [2]	65.28	80.40	85.12	41.29
	PLOT [31]	65.76	81.39	86.73	
<i>VL-Backbones with ReID-domain pre-training:</i>					
P+G	UniPT [37] + IRRA [17]	64.50	80.24	85.74	38.22
	PLIP [54] + IRRA [17]	65.79	81.94	87.32	39.43
	NAM [41] + IRRA ^R	66.34	81.94	86.73	40.14
	NAM [41] + FMFA (ours)	66.58	81.94	87.04	40.17
	HAM [18] + IRRA ^R	68.21	83.28	88.04	41.72
	HAM [18] + FMFA (ours)	68.37	83.28	88.10	41.76

Table 5. Ablation study on each component of FMFA on CUHK-PEDES, ICFG-PEDES and RSTPReid.

No.	Methods	Components			CUHK-PEDES			ICFG-PEDES			RSTPReid		
		SDM	A-SDM	EFA	Rank-1	Rank-5	Rank-10	Rank-1	Rank-5	Rank-10	Rank-1	Rank-5	Rank-10
0	Baseline	✓			73.45	89.38	93.69	63.48	80.16	85.78	59.50	81.80	88.85
1	+A-SDM		✓		74.04	89.86	93.89	64.26	80.59	85.90	60.25	81.45	88.70
2	+EFA	✓		✓	73.73	89.64	94.04	63.77	80.39	85.86	60.45	82.30	89.25
3	FMFA	✓	✓	✓	74.16	90.12	94.10	64.29	80.48	85.93	61.05	83.85	89.80

mAP, which is meaningful for practical applications. When adopting VL-Backbones with ReID-domain pre-training, FMFA yields slight gains, outperforming IRRA by 0.24% and 0.16% in Rank-1 with the NAM-based and HAM-based backbones, respectively.

In summary, our FMFA achieves the best performance across all evaluation metrics on three common public benchmarks. To the best of our knowledge, FMFA is the best method for all global matching methods. This demonstrates the generalizability and robustness of our proposed method.

4.3 Ablation Study

In this section, we analyze our proposed components in the FMFA framework. For simplicity, we omit the components of \mathcal{L}_{id} and the IRR module that were proposed by IRRA and used in all experiments. Only one of SDM and A-SDM can be used at the same time.

To fully demonstrate the impact of our proposed components in FMFA, we conduct an empirical analysis on three common datasets (i.e., CHUK-PEDES [23], ICFG-PEDES [8] and RSTPReid [53]). The Rank-1, Rank-5 and Rank-10 accuracies(%) are shown in Table 5.

Effect of The A-SDM Module. To evaluate the contribution of the Adaptive Similarity Distribution Matching (A-SDM) module, we perform ablation experiments by replacing the A-SDM module with the SDM module, keeping all hyperparameters unchanged. Specifically, as shown in Table 5, replacing A-SDM with SDM leads to a decrease in the Rank-1 accuracy by 0.59%, 0.78%, and 0.75% across the three datasets, as observed in No. 0 vs. No. 1. Additionally, all evaluation metrics on the CUHK-PEDES and ICFG-PEDES datasets degrade, further confirming the superiority of A-SDM. Moreover, when combined with the EFA module, the advantage of A-SDM becomes even more pronounced. As shown in No. 2 vs. No. 3, replacing the A-SDM module with the SDM module

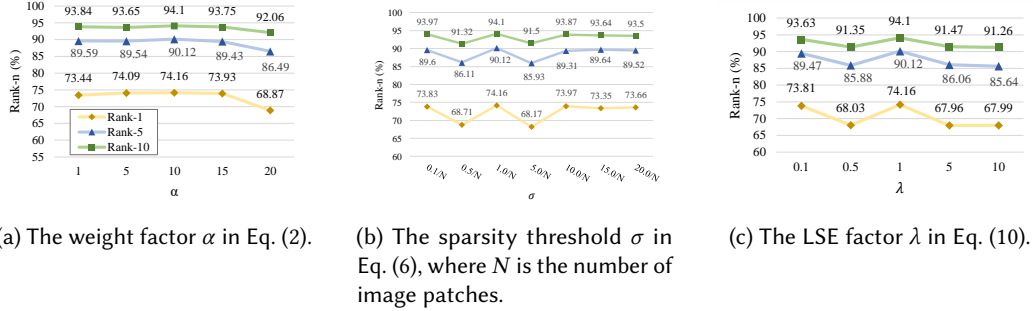


Fig. 4. The sensitivity analysis of hyperparameters of FMFA on the CUHK-PEDES dataset.

results in 1.26% and 1.00% decrease in Rank-1 and Rank-5 on the CUHK-PEDES dataset, respectively, and a 1.55% drop in the Rank-5 accuracy on the RSTPReid dataset. These results collectively validate the consistent and significant contribution of the A-SDM module to overall performance.

Effect of The EFA Module. To enhance the global matching capability of model, the Explicit Fine-grained Alignment (EFA) module introduces fine-grained cross-modal interaction based on a sparse similarity matrix. The effectiveness of the EFA module is demonstrated through the experimental comparisons between No. 0 vs. No. 2 and No. 1 vs. No. 3. Specifically, as shown in No. 1 vs. No. 3, removing the EFA module from FMFA leads to a performance drop of 0.26% and 0.21% in Rank-5 and Rank-10 on the CUHK-PEDES dataset, and a more significant decline of 2.40% and 1.10% in Rank-5 and Rank-10 on the RSTPReid dataset. However, EFA causes a 0.11% drop in Rank-5 on ICFG-PEDES, suggesting that its sparse and hard coding strategy, which focuses only on the most relevant patches, may overlook other informative ones and lead to information loss. Notably, this comparison also reflects the joint ablation of EFA and the A-SDM module, further verifying the complementary effect between the two modules. Moreover, to further validate the individual contribution of the EFA module, we design an additional experiment that retains the SDM module while removing only the EFA module, as observed in No. 0 vs. No. 2. In this setting, the absence of EFA results in 0.38%, 0.29%, and 0.95% drops in Rank-1 on CUHK-PEDES, ICFG-PEDES and RSTPReid, respectively. These comparisons demonstrate the effectiveness of the EFA module.

4.4 Parameter Study

We conduct the parameter analysis on the CUHK-PEDES dataset, including three hyperparameters (i.e., the weight factor α , the sparsity threshold σ and the factor λ) and the weight of the proposed loss functions (i.e., \mathcal{L}_{A-sdm} and \mathcal{L}_{efa}). While we analyze the special parameter, other parameters are kept the same as those described in Section 4.1.

Hyperparameters Analysis. As shown in Figure 4a, we vary the weight factor α from 1 to 20. The results on the CUHK-PEDES dataset indicate that setting α to 10 yields the best performance across all metrics, suggesting that the adaptive pull force on unmatched positive pairs is optimal. However, when α is increased to 20, the performance drops significantly because the pull force becomes excessively strong, causing unmatched positive pairs to fail to align properly and instead over-pulling mismatched positives, which leads to false positives. We further vary the sparsity threshold σ from $0.1/N$ to $20/N$ and the LSE factor λ from 0.1 to 10, where N denotes the number of image patches. As illustrated in Figure 4b and Figure 4c, setting σ to $1/N$ and λ to 1 yields the best overall performance.

Table 6. The sensitivity analysis of the weights of \mathcal{L}_{A-sdm} and \mathcal{L}_{efa} on the CUHK-PEDES dataset.

Weight	\mathcal{L}_{A-sdm}			\mathcal{L}_{efa}		
	Rank-1	Rank-5	Rank-10	Rank-1	Rank-5	Rank-10
0.1	71.47	88.62	93.03	68.32	85.75	91.04
0.5	71.23	88.06	93.16	58.49	80.05	87.13
1.0	74.16	90.12	94.10	74.16	90.12	94.10
5.0	71.86	88.27	93.12	0.09	0.19	0.32
10.0	72.45	88.62	93.24	0.09	0.19	0.32

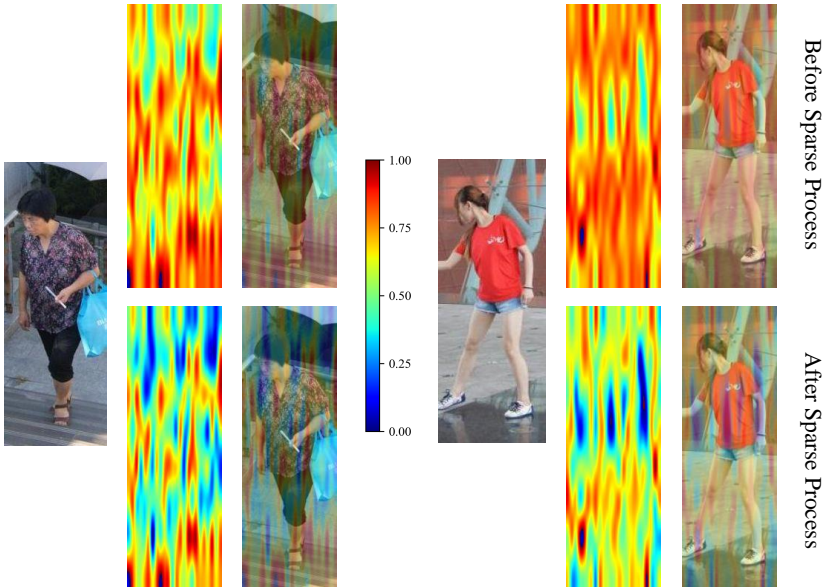


Fig. 5. Visualization of similarity maps before and after the sparse process in the EFA module.

Loss Function Weights. We conduct a series of experiments on the CUHK-PEDES dataset to analyze the effect of the weights of the two proposed loss functions, \mathcal{L}_{A-sdm} and \mathcal{L}_{efa} , varying them from 0.1 to 10.0, as shown in Table 6. The results show that setting both weights to 1 yields the best performance. Notably, increasing the weight of \mathcal{L}_{efa} to 5.0 or 10.0 results in gradient explosion, making the model untrainable and causing all metrics to drop below 1.

4.5 Qualitative Results

Visualization of The Sparse Process. We visualize the similarity maps before and after the sparse process (i.e., Eq. (5) and Eq. (6)) in the EFA module, as shown in Figure 5. Patches with high similarity (greater than 0.75) are preserved, whereas those with low similarity (below 0.5) are suppressed to values under 0.25 and thus omitted during aggregation (left in Figure 5). When most patches in an image exhibit relatively high similarity (around 0.75), the sparse process retains only the patches with the highest similarity, while pushing the similarity of the remaining patches below 0.5 (right in Figure 5). This ensures that the subsequent aggregation focuses only on the most relevant patches, reducing computational and memory costs while maintaining performance. Unlike implicit aggregation methods based on attention mechanisms, EFA explicitly aggregates

Table 7. Comparison of the inference time (s) between FMFA and recent local matching methods.

Method	RSTPReid	CUHK-PEDES	ICFG-PEDES
FMFA (ours)	3	7	50
PLOT [31]	5	16	91
RaSa [2]	388	1168	3871



Fig. 6. Comparison of top-5 retrieved results on CUHK-PEDES between baseline and FMFA for each text query. The image corresponding to query text, along with the matched and mismatched images, are highlighted with black, green and red rectangles, respectively.

image patches and text tokens, allowing us to observe whether the most relevant patches are effectively aggregated by visualizing the similarity between patches and tokens.

Inference Time Comparison We compare the inference time between FMFA and recent local matching methods (e.g., PLOT [31] and RaSa [2]) on the test sets of three datasets, as shown in Table 7. As a global matching method, FMFA only computes global features during inference, thus achieving a higher inference speed than local matching methods. Moreover, the efficiency advantage of FMFA becomes more pronounced as the size of the test set increases. For instance, the inference time of FMFA vs. PLOT increases from 3s vs. 5s on RSTPReid to 50s vs. 91s on ICFG-PEDES.

Visualization of Top-5 Retrieval Results. Figure 6 compares the top-5 retrieval results between the baseline IRR^R and our proposed FMFA on the CUHK-PEDES dataset. As shown in Figure 6, FMFA achieves more accurate retrieval results, successfully retrieving images that the

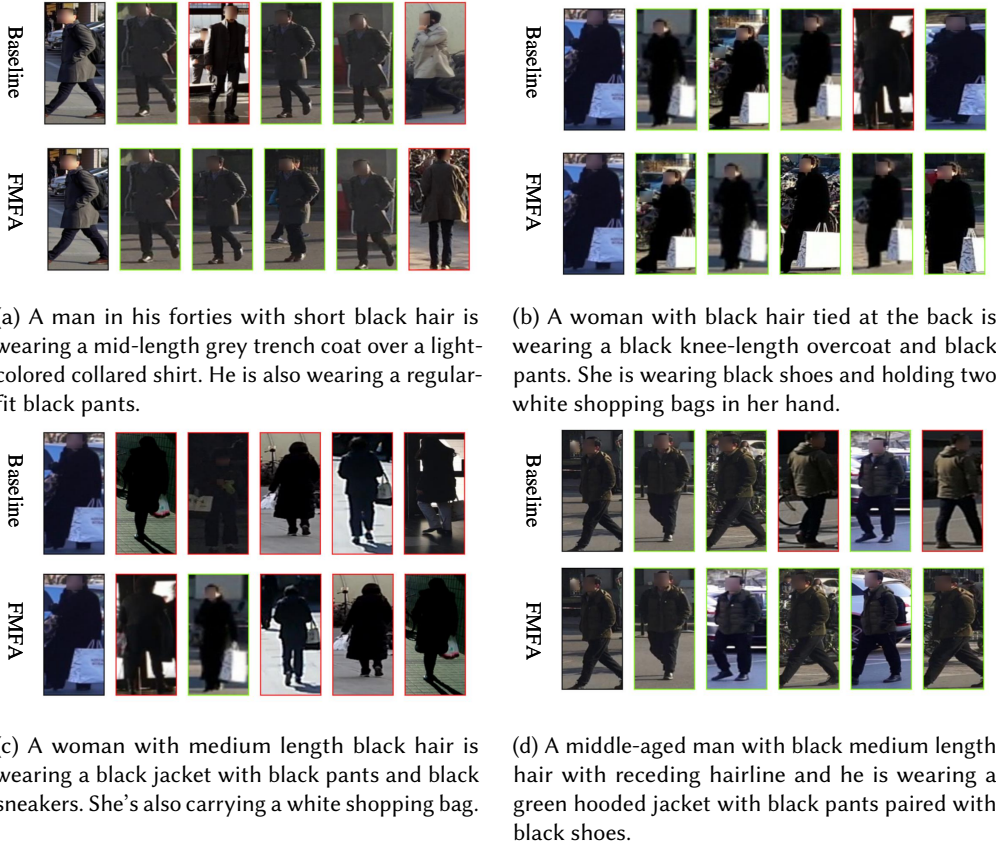


Fig. 7. Comparison of top-5 retrieved results on ICFG-PEDES between baseline and FMFA for each text query. The image corresponding to query text, matched and mismatched images are marked with black, green and red rectangles, respectively.

baseline fails to match. For query texts where the baseline performs well, FMFA further improves performance by retrieving more relevant pedestrian images (e.g., Figure 6a and Figure 6c). Even for hard negative samples, where the baseline struggles to retrieve the correct image, FMFA still enhances the similarity between positive pairs (e.g., Figure 6b and Figure 6d). This is because our proposed FMFA focuses on the unmatched positive pairs and adaptively pulls the positive pairs closer. More comparisons of the top-5 retrieved results between the baseline and FMFA on the ICFG-PEDES and RSTPReid datasets are provided in Figure 7 and Figure 8.

5 Conclusion

In this paper, we propose a cross-modal Full-Mode Fine-grained Alignment (FMFA) framework to learn discriminative global text-image representations through full-mode fine-grained alignment, including explicit fine-grained alignment and existing implicit relational reasoning. We design an Adaptive Similarity Distribution Matching (A-SDM) module to concentrate on unmatched positive pairs, adaptively pulling them closer. In addition, to achieve cross-modal fine-grained alignment, we introduce an Explicit Fine-grained Alignment (EFA) module, which explicitly aggregates local text and image representations based on the sparse similarity matrix and employs a hard coding



Fig. 8. Comparison of top-5 retrieved results on RSTPReid between baseline and FMFA for each text query. The image corresponding to query text, matched and mismatched images are marked with black, green and red rectangles, respectively.

method. These modules work collaboratively to align images and text into a joint embedding space. Extensive experiments on three datasets demonstrate the superiority and effectiveness of our proposed FMFA framework.

Limitation. The fixed threshold in the sparse process only keeps the most relevant patches, which may result in the loss of semantic information and limit the effective aggregation of local features, thereby affecting the overall performance of our model. Incorporating adaptive methods that capture complete semantic information (e.g., tree transformer [43]) could further enhance our model.

Acknowledgments

This work was supported by the National Natural Science Foundation of China (No. 62302080), National Foreign Expert Project of China (No. S20240327), Sichuan Science and Technology Program (No. 2025HJRC0021) and Sichuan Province Innovative Talent Funding Project for Postdoctoral Fellows (No. BX202312).

References

- [1] Jinze Bai, Shuai Bai, Shusheng Yang, Shijie Wang, Sinan Tan, Peng Wang, Junyang Lin, Chang Zhou, and Jingren Zhou. 2023. Qwen-VL: A Versatile Vision-Language Model for Understanding, Localization, Text Reading, and Beyond. *arXiv preprint arXiv:2308.12966* (2023).
- [2] Yang Bai, Min Cao, Daming Gao, Ziqiang Cao, Chen Chen, Zhenfeng Fan, Liqiang Nie, and Min Zhang. 2023. Rasa: Relation and sensitivity aware representation learning for text-based person search. In *Proceedings of the Thirty-Second International Joint Conference on Artificial Intelligence, IJCAI-23*. 555–563.
- [3] Ioana Bica, Anastasija Ilić, Matthias Bauer, Goker Erdogan, Matko Bošnjak, Christos Kaplanis, Alexey A Gritsenko, Matthias Minderer, Charles Blundell, Razvan Pascanu, and Jovana Mitrovic. 2024. Improving fine-grained understanding in image-text pre-training. In *Forty-first International Conference on Machine Learning*.
- [4] Min Cao, Yang Bai, Ziyin Zeng, Mang Ye, and Min Zhang. 2024. An empirical study of clip for text-based person search. In *Proceedings of the AAAI Conference on Artificial Intelligence*, Vol. 38. 465–473.
- [5] Yuxin Chen, Zongyang Ma, Ziqi Zhang, Zhongang Qi, Chunfeng Yuan, Bing Li, Junfu Pu, Ying Shan, Xiaojuan Qi, and Weiming Hu. 2024. How to Make Cross Encoder a Good Teacher for Efficient Image-Text Retrieval?. In *Proceedings of the IEEE/CVF Conference on Computer Vision and Pattern Recognition*. 26994–27003.
- [6] Yuxin Chen, Zongyang Ma, Ziqi Zhang, Zhongang Qi, Chunfeng Yuan, Ying Shan, Bing Li, Weiming Hu, Xiaohu Qie, and Jianping Wu. 2023. Vilem: Visual-language error modeling for image-text retrieval. In *Proceedings of the IEEE/CVF conference on computer vision and pattern recognition*. 11018–11027.
- [7] Jacob Devlin, Ming-Wei Chang, Kenton Lee, and Kristina Toutanova. 2019. Bert: Pre-training of deep bidirectional transformers for language understanding. In *Proceedings of the 2019 conference of the North American chapter of the association for computational linguistics: human language technologies, volume 1 (long and short papers)*. 4171–4186.
- [8] Zefeng Ding, Changxing Ding, Zhiyin Shao, and Dacheng Tao. 2021. Semantically self-aligned network for text-to-image part-aware person re-identification. *arXiv preprint arXiv:2107.12666* (2021).
- [9] Alex Ergasti, Tomaso Fontanini, Claudio Ferrari, Massimo Bertozzi, and Andrea Prati. 2025. MARS: Paying more attention to visual attributes for text-based person search. *ACM Trans. Multimedia Comput. Commun. Appl.* (2025). doi:10.1145/3721482
- [10] Chenyang Gao, Guanyu Cai, Xinyang Jiang, Feng Zheng, Jun Zhang, Yifei Gong, Pai Peng, Xiaowei Guo, and Xing Sun. 2021. Contextual non-local alignment over full-scale representation for text-based person search. *arXiv preprint arXiv:2101.03036* (2021).
- [11] Xiao Han, Sen He, Li Zhang, and Tao Xiang. 2021. Text-based person search with limited data. *arXiv preprint arXiv:2110.10807* (2021).
- [12] Kaiming He, Xinlei Chen, Saining Xie, Yanghao Li, Piotr Dollár, and Ross Girshick. 2022. Masked autoencoders are scalable vision learners. In *Proceedings of the IEEE/CVF conference on computer vision and pattern recognition*. 16000–16009.
- [13] Kaiming He, Xiangyu Zhang, Shaoqing Ren, and Jian Sun. 2016. Deep residual learning for image recognition. In *Proceedings of the IEEE conference on computer vision and pattern recognition*. 770–778.
- [14] David T Hoffmann, Simon Schrödi, Jelena Bratulić, Nadine Behrmann, Volker Fischer, and Thomas Brox. 2024. Eureka-moments in transformers: multi-step tasks reveal softmax induced optimization problems. In *Forty-first International Conference on Machine Learning*.
- [15] Shijuan Huang, Zongyi Li, Hefei Ling, and Jianbo Li. 2025. Cross-Modality Relation and Uncertainty Exploration for Text-Based Person Search. *ACM Transactions on Multimedia Computing, Communications, and Applications* (2025). doi:10.1145/3747185
- [16] Zhong Ji, Junhua Hu, Deyin Liu, Lin Yuanbo Wu, and Ye Zhao. 2022. Asymmetric Cross-Scale Alignment for Text-Based Person Search. *IEEE Transactions on Multimedia* 25 (2022), 7699–7709.
- [17] Ding Jiang and Mang Ye. 2023. Cross-modal implicit relation reasoning and aligning for text-to-image person retrieval. In *Proceedings of the IEEE/CVF Conference on Computer Vision and Pattern Recognition*. 2787–2797.
- [18] Jiayu Jiang, Changxing Ding, Wentao Tan, Junhong Wang, Jin Tao, and Xiangmin Xu. 2025. Modeling Thousands of Human Annotators for Generalizable Text-to-Image Person Re-identification. In *Proceedings of the Computer Vision and Pattern Recognition Conference (CVPR)*. 9220–9230.
- [19] Kuang-Huei Lee, Xi Chen, Gang Hua, Houdong Hu, and Xiaodong He. 2018. Stacked cross attention for image-text matching. In *Proceedings of the European conference on computer vision (ECCV)*. 201–216.
- [20] Junnan Li, Dongxu Li, Silvio Savarese, and Steven Hoi. 2023. Blip-2: Bootstrapping language-image pre-training with frozen image encoders and large language models. In *International conference on machine learning*. 19730–19742.
- [21] Junnan Li, Dongxu Li, Caiming Xiong, and Steven Hoi. 2022. BLIP: Bootstrapping Language-Image Pre-training for Unified Vision-Language Understanding and Generation. In *Proceedings of the 39th International Conference on Machine Learning*. 12888–12900.

[22] Junnan Li, Ramprasaath Selvaraju, Akhilesh Gotmare, Shafiq Joty, Caiming Xiong, and Steven Chu Hong Hoi. 2021. Align before fuse: Vision and language representation learning with momentum distillation. *Advances in neural information processing systems* 34 (2021), 9694–9705.

[23] Shuang Li, Tong Xiao, Hongsheng Li, Bolei Zhou, Dayu Yue, and Xiaogang Wang. 2017. Person search with natural language description. In *Proceedings of the IEEE conference on computer vision and pattern recognition*. 1970–1979.

[24] Haotian Liu, Chunyuan Li, Yuheng Li, Bo Li, Yuanhan Zhang, Sheng Shen, and Yong Jae Lee. 2024. LLaVA-NeXT: Improved reasoning, OCR, and world knowledge. <https://llava-vl.github.io/blog/2024-01-30-llava-next/>

[25] Yating Liu, Zimo Liu, Xiangyuan Lan, Wenming Yang, Yaowei Li, and Qingmin Liao. 2025. Dm-adapter: Domain-aware mixture-of-adapters for text-based person retrieval. In *Proceedings of the AAAI Conference on Artificial Intelligence*. 5703–5711.

[26] Francesco Locatello, Dirk Weissenborn, Thomas Unterthiner, Aravindh Mahendran, Georg Heigold, Jakob Uszkoreit, Alexey Dosovitskiy, and Thomas Kipf. 2020. Object-centric learning with slot attention. *Advances in neural information processing systems* 33 (2020), 11525–11538.

[27] Jiasen Lu, Dhruv Batra, Devi Parikh, and Stefan Lee. 2019. Vilbert: Pretraining task-agnostic visiolinguistic representations for vision-and-language tasks. *Advances in neural information processing systems* 32 (2019), 13–23.

[28] Zefeng Lu, Ronghao Lin, Yap-Peng Tan, and Haifeng Hu. 2025. Prompt-guided Transformer and MLLM Interactive Learning for Text-Based Pedestrian Search. *IEEE Transactions on Information Forensics and Security* 20 (2025), 7181–7196.

[29] Jishnu Mukhoti, Tsung-Yu Lin, Omid Poursaeed, Rui Wang, Ashish Shah, Philip H. S. Torr, and Ser-Nam Lim. 2023. Open vocabulary semantic segmentation with patch aligned contrastive learning. In *Proceedings of the IEEE/CVF Conference on Computer Vision and Pattern Recognition*. 19413–19423.

[30] Aaron van den Oord, Yazhe Li, and Oriol Vinyals. 2018. Representation learning with contrastive predictive coding. *arXiv preprint arXiv:1807.03748* (2018).

[31] Jicheol Park, Dongwon Kim, Boseung Jeong, and Suha Kwak. 2024. PLOT: Text-Based Person Search with Part Slot Attention for Corresponding Part Discovery. In *European Conference on Computer Vision*. 474–490.

[32] Yang Qin, Yingke Chen, Dezhong Peng, Xi Peng, Joey Tianyi Zhou, and Peng Hu. 2024. Noisy-correspondence learning for text-to-image person re-identification. In *Proceedings of the IEEE/CVF Conference on Computer Vision and Pattern Recognition*. 27197–27206.

[33] Alec Radford, Jong Wook Kim, Chris Hallacy, Aditya Ramesh, Gabriel Goh, Sandhini Agarwal, Girish Sastry, Amanda Askell, Pamela Mishkin, Jack Clark, Gretchen Krueger, and Ilya Sutskever. 2021. Learning transferable visual models from natural language supervision. In *International conference on machine learning*. 8748–8763.

[34] Robin Rombach, Andreas Blattmann, Dominik Lorenz, Patrick Esser, and Björn Ommer. 2022. High-Resolution Image Synthesis with Latent Diffusion Models. In *2022 IEEE/CVF Conference on Computer Vision and Pattern Recognition (CVPR)*. 10674–10685.

[35] Florian Schroff, Dmitry Kalenichenko, and James Philbin. 2015. Facenet: A unified embedding for face recognition and clustering. In *Proceedings of the IEEE conference on computer vision and pattern recognition*. 815–823.

[36] Rico Sennrich, Barry Haddow, and Alexandra Birch. 2016. Neural machine translation of rare words with subword units. In *Proceedings of the 54th Annual Meeting of the Association for Computational Linguistics (Volume 1: Long Papers)*. 1715–1725.

[37] Zhiyin Shao, Xinyu Zhang, Changxing Ding, Jian Wang, and Jingdong Wang. 2023. Unified Pre-training with Pseudo Texts for Text-To-Image Person Re-identification. In *2023 IEEE/CVF International Conference on Computer Vision (ICCV)*. 11140–11150.

[38] Zhiyin Shao, Xinyu Zhang, Meng Fang, Zhifeng Lin, Jian Wang, and Changxing Ding. 2022. Learning granularity-unified representations for text-to-image person re-identification. In *Proceedings of the 30th acm international conference on multimedia*. 5566–5574.

[39] Xiujun Shu, Wei Wen, Haoqian Wu, Keyu Chen, Yiran Song, Ruizhi Qiao, Bo Ren, and Xiao Wang. 2022. See finer, see more: Implicit modality alignment for text-based person retrieval. In *European Conference on Computer Vision*. 624–641.

[40] Naoya Sogi, Takashi Shibata, and Makoto Terao. 2024. Object-Aware Query Perturbation for Cross-Modal Image-Text Retrieval. In *European Conference on Computer Vision*. 447–464.

[41] Wentao Tan, Changxing Ding, Jiayu Jiang, Fei Wang, Yibing Zhan, and Dapeng Tao. 2024. Harnessing the Power of MLLMs for Transferable Text-to-Image Person ReID. In *2024 IEEE/CVF Conference on Computer Vision and Pattern Recognition (CVPR)*. 17127–17137.

[42] Wilson L. Taylor. 1953. “Cloze procedure”: A new tool for measuring readability. *Journalism quarterly* 30, 4 (1953), 415–433.

[43] Yaushian Wang, Hung-yi Lee, and Yun-Nung Chen. 2019. Tree Transformer: Integrating Tree Structures into Self-Attention. In *Proceedings of the 2019 Conference on Empirical Methods in Natural Language Processing and the 9th International Joint Conference on Natural Language Processing (EMNLP-IJCNLP)*. 1061–1070.

- [44] Zhe Wang, Zhiyuan Fang, Jun Wang, and Yezhou Yang. 2020. Vitaa: Visual-textual attributes alignment in person search by natural language. In *Computer vision–ECCV 2020: 16th European conference, glasgow, UK, August 23–28, 2020, proceedings, part XII 16*. 402–420.
- [45] Zhimin Wei, Zhipeng Zhang, Peng Wu, Ji Wang, Peng Wang, and Yanning Zhang. 2024. Fine-Granularity Alignment for Text-Based Person Retrieval Via Semantics-Centric Visual Division. *IEEE Transactions on Circuits and Systems for Video Technology* 34, 9 (2024), 8242–8252.
- [46] Tinghui Wu, Shuhe Zhang, Dihu Chen, and Haifeng Hu. 2024. Text-and-Image Learning Transformer for Cross-Modal Person Re-Identification. *ACM Transactions on Multimedia Computing, Communications, and Applications* 21, 1 (2024), 1–18.
- [47] Shuanglin Yan, Neng Dong, Liyan Zhang, and Jinhui Tang. 2023. Clip-driven fine-grained text-image person re-identification. *IEEE Transactions on Image Processing* 32 (2023), 6032–6046.
- [48] Shuanglin Yan, Hao Tang, Liyan Zhang, and Jinhui Tang. 2023. Image-specific information suppression and implicit local alignment for text-based person search. *IEEE transactions on neural networks and learning systems* 35, 12 (2023), 17973–17986.
- [49] Shuyu Yang, Yinan Zhou, Zhedong Zheng, Yaxiong Wang, Li Zhu, and Yujiao Wu. 2023. Towards Unified Text-based Person Retrieval: A Large-scale Multi-Attribute and Language Search Benchmark. In *Proceedings of the 31st ACM international conference on multimedia*. 4492–4501.
- [50] Lewei Yao, Runhui Huang, Lu Hou, Guansong Lu, Minzhe Niu, Hang Xu, Xiaodan Liang, Zhenguo Li, Xin Jiang, and Chunjing Xu. 2022. Filip: Fine-grained interactive language-image pre-training. In *International Conference on Learning Representations*.
- [51] Ying Zhang and Huchuan Lu. 2018. Deep cross-modal projection learning for image-text matching. In *Proceedings of the European conference on computer vision (ECCV)*. 686–701.
- [52] Zhedong Zheng, Liang Zheng, Michael Garrett, Yi Yang, Mingliang Xu, and Yi-Dong Shen. 2020. Dual-path convolutional image-text embeddings with instance loss. *ACM Transactions on Multimedia Computing, Communications, and Applications* 16, 2 (2020), 1–23.
- [53] Aichun Zhu, Zijie Wang, Yifeng Li, Xili Wan, Jing Jin, Tian Wang, Fangqiang Hu, and Gang Hua. 2021. Dssl: Deep surroundings-person separation learning for text-based person retrieval. In *Proceedings of the 29th ACM international conference on multimedia*. 209–217.
- [54] Jialong Zuo, Jiahao Hong, Feng Zhang, Changqian Yu, Hanyu Zhou, Changxin Gao, Nong Sang, and Jingdong Wang. 2024. PLIP: Language-Image Pre-training for Person Representation Learning. *Advances in Neural Information Processing Systems* 37 (2024), 45666–45702.

Received 12 August 2025; revised XX XXX 2025; accepted XX XXX 2025